Microscopic description of triaxiality in Ru isotopes with covariant energy density functional theory

Z. Shi (施智)[1] and Z. P. Li (李志攀)[2,*]

[1]*School of Physics and Nuclear Energy Engineering, Beihang University, Beijing 100191, China*

[2]*School of Physical Science and Technology, Southwest University, Chongqing 400715, China*

(Received 11 December 2017; revised manuscript received 12 February 2018; published 29 March 2018)

Background: Triaxiality in nuclear low-lying states has attracted great interest for many years. Recently, reduced transition probabilities for levels near the ground state in ^{110}Ru have been measured and provided strong evidence of a triaxial shape of this nucleus.

Purpose: The aim of this work is to provide a microscopic study of low-lying states for Ru isotopes with $A \approx 100$ and to examine in detail the role of triaxiality and the evolution of quadrupole shapes with the isospin and spin degrees of freedom.

Method: Low-lying excitation spectra and transition probabilities of even-even Ru isotopes are described at the beyond-mean-field level by solving a five-dimensional collective Hamiltonian with parameters determined by constrained self-consistent mean-field calculations based on the relativistic energy density functional PC-PK1.

Results: The calculated energy surfaces, low-energy spectra, and intraband and interband transition rates, as well as some characteristic collective observables, such as $E(4^+_{\rm g.s.})/E(2^+_{\rm g.s.})$, $E(2^+_\gamma)/E(4^+_{\rm g.s.})$, and $B(E2; 2^+_{\rm g.s.} \rightarrow 0^+_{\rm g.s.})$ and γ-band staggerings, are in good agreement with the available experimental data.

Conclusions: The main features of the experimental low-lying excitation spectra and electric transition rates are well reproduced and, thus, strongly support the onset of triaxiality in the low-lying excited states of Ru isotopes around ^{110}Ru.

DOI: 10.1103/PhysRevC.97.034329

I. INTRODUCTION

Triaxial deformation in the atomic nucleus is related to many interesting phenomena, such as wobbling motion [1] and nuclear chirality [2,3]. The observation of chiral doublet bands [4] and wobbling bands [5] provides direct evidence of the existence of triaxial deformation. Recently, not only the static triaxial deformation, but also the triaxial shape transition along, e.g., the increasing neutron numbers, has attracted a lot of attention [6–15].

Due to the subtle interplay between single-particle and collective degrees of freedom, the evolution of triaxiality in the $A \approx 100$ mass region has been a hot topic for years; one example is the ruthenium isotopes. In past decades, many experimental and theoretical efforts have been reported. In the 1980s, multiple Coulomb excitation experiments on ^{104}Ru, which is the heaviest stable Ru isotope, have suggested a phase transition from a spherical to a soft triaxial rotor rather than to an axially symmetric rotor with increasing neutron number in Ru isotopes [16]. Later, through the β decays of Tc isotopes, the low-lying collective structures of ^{106,108}Ru [17] and ^{110,112}Ru [18] were studied, which suggested the importance of triaxial deformation in all these nuclei and demonstrated a trend toward increasing triaxial rigidity with more neutrons. Furthermore, the high-spin structures in these neutron-rich Ru isotopes have been extensively studied by fusion-fission reactions [19] and spontaneous fissions of ^{248}Cm [20] and ^{252}Cf [21,22]. In Ref. [22], a pair of $\Delta I = 1$ negative-parity doublet bands was observed in ^{110}Ru and ^{112}Ru. They were interpreted as soft chiral vibrations. Very recently, a multistep Coulomb excitation measurement following the postacceleration of an unstable ^{110}Ru beam was performed and the newly measured reduced transition probabilities provided direct evidence of a relatively rigid triaxial shape near the ground state in ^{110}Ru [23].

Theoretically, various methods [15,24–33] have been devoted to investigating the evolution of triaxiality in Ru isotopes. Using the macroscopic-microscopic finite-range liquid-drop model, Möller *et al.* have identified ^{108}Ru as having the largest effects of triaxial deformation, ∼0.7 MeV, on the ground-state energy [24,25]. In the interacting boson model (IBM), γ-soft behaviors are found for Ru isotopes around $A \approx 100$, but no candidates for a triaxial ground state are found [26,27]. Within the framework of the cranked shell model with the nonaxial deformed Woods-Saxon potential, the ground states of ^{108,110,112}Ru are found to be triaxial, and ^{112}Ru is the softest in the γ direction. It is also found that the ground state of ^{114}Ru is oblate [28]. The potential energy surfaces (PESs) obtained from the Skyrme Hartree-Fock calculations show triaxial shapes for the ground states of $^{108-114}$Ru, which become more rigid with increasing neutron number [29]. While the PESs obtained from the Hartree-Fock-Bogoliubov (HFB) with Gogny functional D1M predict triaxial ground-state shapes for $^{104-114}$Ru, and γ-soft behaviors are found, in which ^{104}Ru is the softest in the γ direction [15]. In Ref. [31], a

*zpliphy@swu.edu.cn

prolate-triaxial-oblate shape transition is found for the isotopes $^{96-112}$Ru by the relativistic Hartree-Bogoliubov (RHB) calculations with DD-PC1 and DD-ME2; the ground states of ^{110,112}Ru are oblate with clearly triaxial softness. A recent investigation of band structures in ^{108,110,112}Ru with two complementary theoretical models, the cranked HFB method with density functional UNEDF0 and the triaxial projected shell model, concludes that the high-spin behavior in ^{108,110,112}Ru consists of triaxial rotation, while the obtained triaxial minima are fairly shallow [32]. Very recently, the band structure in these even Ru isotopes was also investigated in the framework of the effective field theory [33].

Despite numerous efforts, it is clear that more studies are necessary to draw an unambiguous conclusion on the detail of triaxial shape transition in neutron-rich Ru isotopes. On the other hand, the increasing data in this mass region accumulated by the modern experimental techniques could provide a stringent examination for various theoretical models.

The microscopic density functional theory, which starts from an effective nucleon-nucleon interaction and self-consistently determines the nuclear mean field by all the independent particles inside, has achieved a lot of success in describing the properties of both nuclear ground states and excitation states. The covariant density functional theory (CDFT) [34–38] embeds the fundamental Lorentz invariance from the very beginning and naturally includes the spin-orbit interaction [39–42], which proves to be a successful theory used over the whole nuclide chart, from relatively light systems to superheavy nuclei [36,43–46], from the valley of β stability to the drip lines [36,47–50], and from collective rotations to collective vibrations [51–58]. One of the most successful density functionals is PC-PK1 [45], which could provide a good description of the isospin dependence of nuclear properties, such as mass [45,59] and quadrupole moments [60].

To take into account the beyond-mean-field effects and describe the low-lying states, in the past few years, the five-dimensional collective Hamiltonian based on CDFT (5DCH-CDFT) has been developed [61–63] and achieved great success for nuclei ranging from light to superheavy mass regions [64], including spherical [65,66], transitional [8,11,14,67–71], and well-deformed [61,62,72] ones. The approach of the collective Hamiltonian has also been applied to chiral [73,74] and wobbling [74–76] motions. In the $A \approx 100$ mass region, the triaxial structures in the Mo isotopes, the neighboring even element of Ru, and the $N = 60$ isotones have been investigated with the 5DCH-CDFT [14]. It is found that the evolution of nuclear collectivity is governed by the novel triaxial structure in which the triaxiality serves as a tunnel from the weakly deformed oblate shape to the largely deformed prolate shape [14].

To provide a new survey of the shape transitions in Ru isotopes and a microscopic description of the recent experimental data, in this paper we present 5DCH-CDFT studies of even-even $^{100-114}$Ru isotopes based on the density functional PC-PK1. A systematic analysis that includes collective potential energy surfaces, low-energy collective spectra, electric transition rates, γ-band staggerings, and collective wave functions is carried out.

II. THEORETICAL FRAMEWORK

The detailed formalism of the 5DCH has been presented in a number of publications (see, e.g., Refs. [61,77,78]). For completeness, a brief introduction is presented here. The 5DCH, which can simultaneously treat quadrupole vibrational and rotational excitations, is expressed in terms of the two deformation parameters β and γ and three Euler angles $(\phi,\theta,\psi) \equiv \Omega$ that define the orientation of the intrinsic principal axes in the laboratory frame,

$$\hat{H}_{\rm coll}(\beta,\gamma) = \hat{T}_{\rm vib}(\beta,\gamma) + \hat{T}_{\rm rot}(\beta,\gamma,\Omega) + V_{\rm coll}(\beta,\gamma). \quad (1)$$

The three terms in $\hat{H}_{\rm coll}(\beta,\gamma)$ are the vibrational kinetic energy,

$$\hat{T}_{\rm vib} = -\frac{\hbar^2}{2\sqrt{wr}}\left\{\frac{1}{\beta^4}\left[\frac{\partial}{\partial\beta}\sqrt{\frac{r}{w}}\beta^4 B_{\gamma\gamma}\frac{\partial}{\partial\beta} - \frac{\partial}{\partial\beta}\sqrt{\frac{r}{w}}\beta^3 B_{\beta\gamma}\frac{\partial}{\partial\gamma}\right]\right.$$
$$+\frac{1}{\beta\sin 3\gamma}\left[-\frac{\partial}{\partial\gamma}\sqrt{\frac{r}{w}}\sin 3\gamma\, B_{\beta\gamma}\frac{\partial}{\partial\beta}\right.$$
$$\left.\left.+\frac{1}{\beta}\frac{\partial}{\partial\gamma}\sqrt{\frac{r}{w}}\sin 3\gamma\, B_{\beta\beta}\frac{\partial}{\partial\gamma}\right]\right\}, \quad (2)$$

the rotational kinetic energy,

$$\hat{T}_{\rm rot} = \frac{1}{2}\sum_{k=1}^{3}\frac{\hat{J}_k^2}{\mathcal{I}_k}, \quad (3)$$

and the collective potential, $V_{\rm coll}$, respectively. Here, $\hat{J}_k$ denote the components of the total angular momentum in the body-fixed frame, and both the mass parameters $B_{\beta\beta}$, $B_{\beta\gamma}$, $B_{\gamma\gamma}$ and the moments of inertia $\mathcal{I}_k$ depend on the quadrupole deformation variables β and γ. Two additional quantities that appear in the $\hat{T}_{\rm vib}$ term, $r = B_1B_2B_3$ and $w = B_{\beta\beta}B_{\gamma\gamma} - B_{\beta\gamma}^2$, determine the volume element in the collective space.

The eigenvalue problem of Hamiltonian (1) is solved using an expansion of eigenfunctions in terms of a complete set of basis functions that depend on the five collective coordinates β, γ, and $\Omega(\phi,\theta,\psi)$ [61]. Using the collective wave functions thus obtained,

$$\Psi_\alpha^{IM}(\beta,\gamma,\Omega) = \sum_{K\in\Delta I}\psi_{\alpha K}^I(\beta,\gamma)\Phi_{MK}^I(\Omega), \quad (4)$$

various observables such as the $E2$ transition probabilities can be calculated,

$$B(E2;\alpha I \to \alpha' I') = \frac{1}{2I+1}|\langle\alpha' I'||\hat{M}(E2)||\alpha I\rangle|^2, \quad (5)$$

where $\hat{M}(E2)$ is the electric quadrupole operator.

In the framework of 5DCH-CDFT, the collective parameters of 5DCH, including the mass parameters $B_{\beta\beta}$, $B_{\beta\gamma}$, and $B_{\gamma\gamma}$, the moments of inertia $\mathcal{I}_k$, and the collective potential $V_{\rm coll}$, are all determined microscopically from the constrained triaxial CDFT calculations. The moments of inertia are calculated with the Inglis-Beliaev formula [79,80], and the mass parameters with the cranking approximation [81]. The collective potential $V_{\rm coll}$ is obtained by subtracting the zero-point energy corrections [81] from the total energy that corresponds to the solution of the constrained triaxial CDFT. The detailed formalism can be found in Ref. [61].

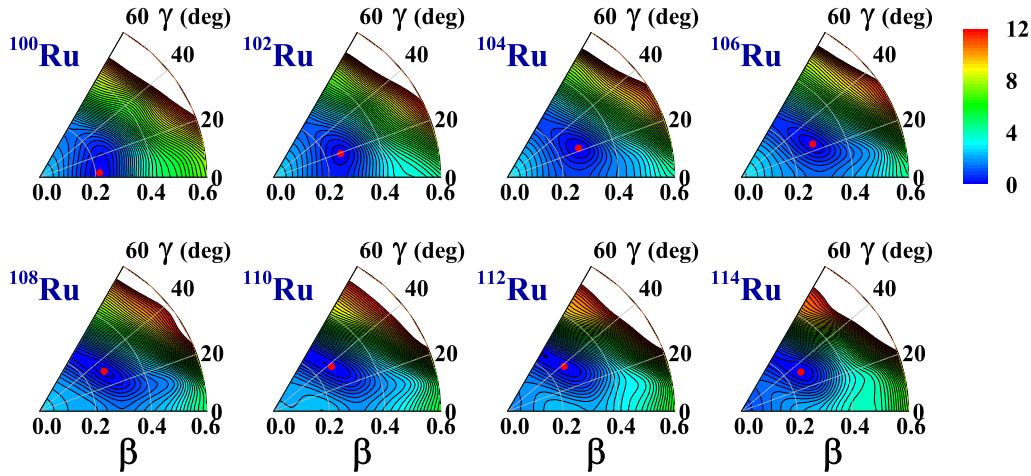

FIG. 1. Potential energy surfaces of even-even $^{100-114}$Ru isotopes in the β-γ plane calculated by the constrained triaxial RMF + BCS with the PC-PK1 functional. All energies are normalized with respect to the binding energy of the absolute minimum (indicated by a red circle). The energy difference between the neighboring contour lines is 0.25 MeV.

III. RESULTS AND DISCUSSION

In the present work, we focus on even Ru isotopes with a neutron number from $N = 54$ to $N = 70$. To determine the collective parameters in the 5DCH, we perform the constrained triaxial CDFT calculations; the pairing correlations are treated using the BCS method. In the particle-hole channel, the point-coupling density functional PC-PK1 [45] is used, and a density-independent δ force is used in the particle-particle channel. The strength parameter of the δ force is 349.5 MeV fm^3 (330.0 MeV fm^3) for neutrons (protons) [45]. The Dirac equation is solved by expanding the Dirac spinor in terms of the three-dimensional harmonic oscillator basis with 12 major shells.

A. Potential energy surfaces and binding energies

Figure 1 displays the PESs of even-even $^{100-114}$Ru isotopes in the β-γ plane. The quadrupole deformations (β, γ) that correspond to the global minima are listed in Table I, as are the energy differences of $\Delta E_{\rm tri}$. In the following, we denote this energy difference the triaxial deformation energy. $\Delta E_{\rm tri}$ is defined as the energy difference of the global minimum with respect to the lowest energy under axial symmetry. Starting from the nearly prolate ^{100}Ru, where the global minimum is located at (0.22,4°), a considerable triaxial deformation, $\gamma = 19°$, is predicted in the global minimum of ^{102}Ru with only two more neutrons. The PES of ^{102}Ru is rather soft along the γ direction at $|\Delta E_{\rm tri}| = 0.324$ MeV. The patterns of the PESs in ^{104,106}Ru are similar, with remarkable triaxiality, $\gamma > 20°$ and $|\Delta E_{\rm tri}| > 0.6$ MeV. For $N \geqslant 64$, the deformations of the global minima of ^{108}Ru, ^{110}Ru, ^{112}Ru, and ^{114}Ru are (0.27,32°), (0.26,37°), (0.26,38°), and (0.25,34°), respectively. The PESs of these four nuclei are very flat along the γ direction towards the oblate side but relatively rigid towards the prolate side. It is also noted that a local spherical minimum emerges in ^{114}Ru.

TABLE I. Quadrupole deformations (β, γ) of the global minima and triaxial deformation energies $\Delta E_{\rm tri}$ for $^{100-114}$Ru calculated by CDFT with PC-PK1. $E_{\rm tri}$ is the total energy for the global minima, and $E_{\rm axi}$ is the lowest energy under axial symmetry.

Nucleus	(β,γ)	$E_{\rm tri}$ (MeV)	$E_{\rm axi}$ (MeV)	$\Delta E_{\rm tri}$ (MeV)
^{100}Ru	(0.21,4°)	−858.425	−858.421	−0.004
^{102}Ru	(0.25,19°)	−874.342	−874.018	−0.324
^{104}Ru	(0.27,22°)	−889.607	−888.739	−0.868
^{106}Ru	(0.28,25°)	−904.040	−903.364	−0.676
^{108}Ru	(0.27,32°)	−917.718	−917.408	−0.310
^{110}Ru	(0.26,37°)	−930.674	−930.601	−0.073
^{112}Ru	(0.26,38°)	−942.767	−942.712	−0.055
^{114}Ru	(0.25,33°)	−953.971	−953.611	−0.360

As mentioned above, similar topograghies of the PESs in Ru isotopes have also been obtained in studies based on the RHB with density functionals DD-ME2 and DD-PC1 [31] and the HFB with the Gogny-D1M density functional [15]. Some differences can be found in the exact locations of the equilibrium triaxial minima and the corresponding triaxial deformation energies. The ground states of ^{110,112}Ru are oblate in the RHB calculations with both the DD-ME2 and the DD-PC1 functionals [31]. In the HFB calculation with Gogny-D1M, only $^{104-108}$Ru are triaxiality deformed in the ground states. The shape coexistence in ^{114}Ru is not observed in the HFB calculation either [15].

In Figs. 2(a) and 2(b), we compare the theoretical binding energies and two-neutron separation energies calculated by the triaxial CDFT and the 5DCH to the experimental data for Ru isotopes. For the mean-field calculations, the deviations of the binding energies from the data are in the range 2.0–3.5 MeV. It is remarkable that the deviations are reduced to be within 1.6 MeV by considering the dynamical correlations associated with rotational motion and quadrupole shape vibrational motion in the 5DCH calculations. This is consistent with a global study of dynamic correlation energies for 575 even-even nuclei using the 5DCH based on the PC-PK1 functional [88,89]. In the global study in Refs. [88] and [89], after taking into account these dynamic correlation energies, the root-mean-square deviation of the nuclear masses is reduced significantly,

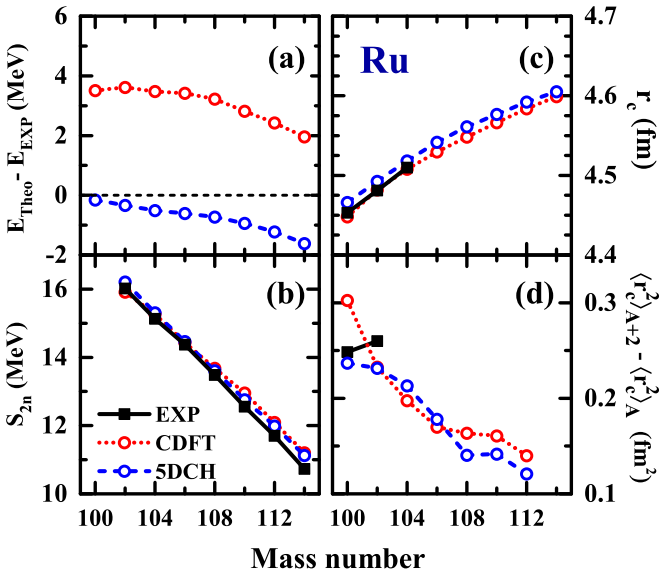

FIG. 2. (a) Deviations of the binding energies calculated by the triaxial CDFT and 5DCH from the data for Ru isotopes. Evolution of (b) the theoretical two-neutron separation energies S_{2n}, (c) the root-mean-square charge radii r_c, and (d) the isotope shifts of the ground-state charge radii $\langle r_c^2\rangle_{A+2} - \langle r_c^2\rangle_A$ as functions of the mass number in Ru isotopes, in comparison with available data [82,83].

from 2.52 to 1.14 MeV [89]. The description of two-neutron separation energies is slightly modified by the 5DCH; both the mean-field and the 5DCH results are in good agreement with the data.

In Figs. 2(c) and 2(d), the charge radii r_c and isotope shifts of the ground-state charge radii $\langle r_c^2\rangle_{A+2} - \langle r_c^2\rangle_A$ as functions of the mass number in Ru isotopes are shown. The charge radii calculated by CDFT are in good agreement with the available data and increase smoothly with the mass number. Similar results are obtained with 5DCH, but the values are slightly larger than those with CDFT because of the beyond-mean-field effect [78]. The theoretical isotope shifts decrease gradually as the mass number increases; that is, the increasing trend of charge radii becomes slow because of the saturation of quadrupole deformations (cf. Fig. 1 and Table I).

B. Low-energy collective spectra

Starting from constrained self-consistent solutions, the collective parameters that determine 5DCH are calculated as functions of the deformation parameters β and γ. The diagonalization of the resulting Hamiltonian yields the excitation energies and collective wave functions.

Figure 3 displays the collective excitation spectra, including the ground-state bands and γ bands, in even-even $^{100-114}$Ru isotopes calculated by the 5DCH-CDFT, in comparison with the available experimental data. The intraband and interband $B(E2)$ values are also shown in the figure. It is noted that the inertia parameters in the present study are calculated by the Inglis-Beliaev formula, which do not include the Thouless-Valatin dynamical rearrangement contributions and, thus, would systematically underestimate the empirical values. As illustrated in Ref. [90], the Thouless-Valatin corrections are almost independent of deformation, and therefore, for a given nucleus the effective moment of inertia used in the collective Hamiltonian can simply be obtained by renormalizing the Inglis-Beliaev values with a constant factor, which is determined by reproducing the excitation energy of the 2_1^+ state [61].

The levels are grouped into ground-state (g.s.) bands and γ bands (γ) according to the predominant K components and dominant decay patterns. For the stable nuclei ^{100,102}Ru, the 5DCH calculations can reproduce the collective structure, although the theoretical spectra are stretched and the intraband transitions are generally larger. This may be due to the overestimation of the collectivity of these two isotopes in the calculations. Starting from ^{104}Ru, the 5DCH calculations are in very good agreement with the experimental data for both excitation energies and transition rates. In particular, the signatures of the triaxiality including the low-lying γ bandhead, the enhanced interband transitions between the γ band and the ground-state band, the γ-band staggerings (cf. Fig. 6), and the relations $E(3_\gamma^+) \approx E(2_{\text{g.s.}}^+) + E(2_\gamma^+)$ [91], are all reproduced very well.

Very recently, the reduced transition probabilities obtained for levels near the ground state of ^{110}Ru have been measured and provided strong evidence of a triaxial shape of this nucleus [23]. As shown in Fig. 4, the measured intraband and interband $B(E2)$ values of ^{110}Ru are consistent with our 5DCH calculations with both the PC-PK1 [45] and the DD-PC1 [85] functionals and, also, the mapped IBM calculation [15]. It should be emphasized that in the 5DCH model, the transition probabilities are calculated in a full configuration space and there are no effective charges used. Therefore, the agreements between the present calculations and the experimental data are very remarkable. Moreover, the excitation energies predicted by both the PC-PK1 and the DD-PC1 functionals are also in very good agreement with the data. Combining the calculated PES, low-energy spectrum, and $E2$ transition rates of ^{110}Ru, the triaxiality near the ground state of ^{110}Ru is further supported.

Furthermore, in Fig. 5 we analyze the evolution of some characteristic collective observables, such as the $E(4_{\text{g.s.}}^+)/E(2_{\text{g.s.}}^+)$, $E(2_\gamma^+)/E(4_{\text{g.s.}}^+)$, and $B(E2; 2_{\text{g.s.}}^+ \to 0_{\text{g.s.}}^+)$ values with the mass number of Ru isotopes calculated by the 5DCH-CDFT, in comparison with the available data [84] and theoretical results from the mapped IBM [15]. The measured $E(4_{\text{g.s.}}^+)/E(2_{\text{g.s.}}^+)$ values vary from $\sim$2.3 to $\sim$2.7, indicating that the Ru isotopes are located in a transitional region. However, for ^{100,102}Ru, the theoretical results calculated by both the 5DCH and the mapped IBM are too large. This is probably because both calculations overestimate the collectivity of these nuclei. For heavier isotopes, the experimental values of $E(4_{\text{g.s.}}^+)/E(2_{\text{g.s.}}^+)$ are reproduced by the 5DCH and mapped IBM quite well.

For a nucleus with considerable triaxial deformation, the γ bandhead 2_γ^+ is generally lower than the $4_{\text{g.s.}}^+$ state, and this is fulfilled for $^{110-114}$Ru according to the measurement in Fig. 5(b). The values of $E(2_\gamma^+)/E(4_{\text{g.s.}}^+)$ calculated with the 5DCH are in reasonable agreement with the data, and the possible triaxial deformation is predicted to start from

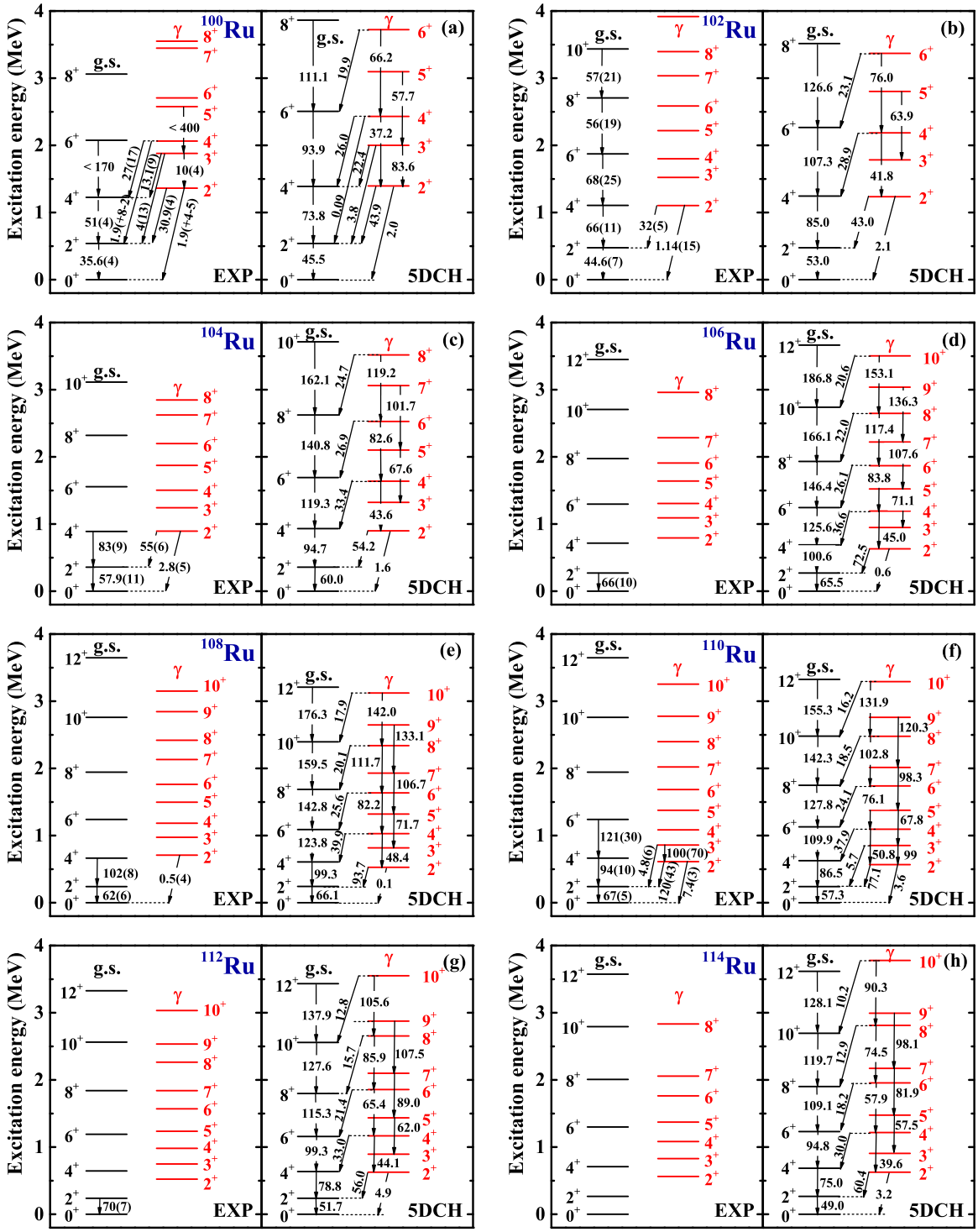

FIG. 3. Calculated excitation energies (in MeV) and intraband and interband $B(E2)$ values (in W.u.) for ground-state bands and γ bands in even-even $^{100-114}$Ru isotopes by 5DCH-CDFT, in comparison with the experimental data (see [86]) [23,84].

^{106}Ru. This is similar to the calculations from the mapped IBM, but for ^{100,102}Ru, the mapped IBM overestimates the data significantly. This is due to the fact that the IBM model space, comprising only a finite number of s and d bosons, is not large enough to describe the energy levels near the closed shell [15]. The comparison of $B(E2; 2^+_{\rm g.s.} \to 0^+_{\rm g.s.})$ among the 5DCH, the mapped IBM [15], and the experimental data are shown in Fig. 5(c). The experimental $B(E2; 2^+_{\rm g.s.} \to 0^+_{\rm g.s.})$ increases gradually till $A = 106$ and saturates for heavier isotopes. Without any effective charges, the 5DCH can reproduce the experimental data very well, except for $A \geqslant 110$, where the theoretical results decrease with the mass number. On the other hand, the results from the mapped IBM are overall smaller than the data.

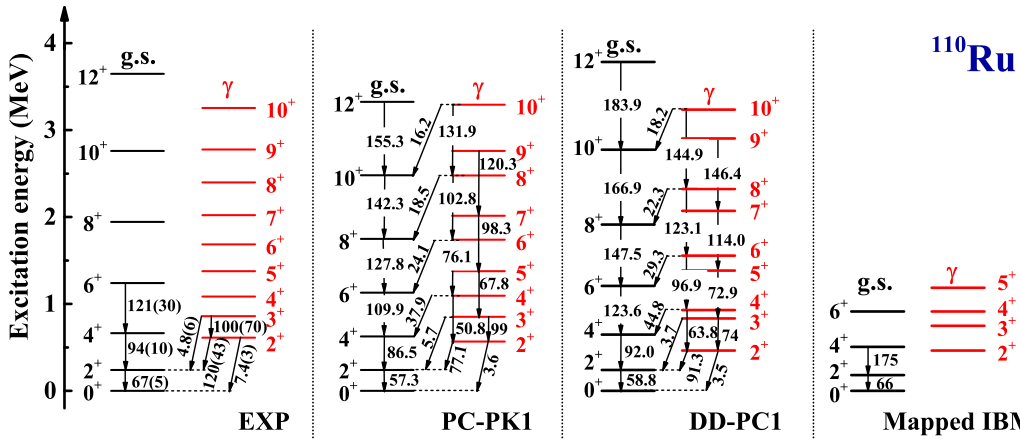

FIG. 4. Energy spectra for ^{110}Ru calculated by 5DCH-CDFT with PC-PK1 [45] and DD-PC1 [85], in comparison with the available mapped IBM results [15] and experimental data [23,84]. In the calculation with DD-PC1, a separable pairing [87] is adopted.

The γ-band staggering parameter

$$S(I) = \frac{[E(I) - E(I-1)] - [E(I-1) - E(I-2)]}{E(2_1^+)}$$

is an indicator of the triaxial softness/rigidity [92]. For a nucleus with a deformed γ-soft potential, $S(I)$ oscillates between negative values for even-spin states and positive values for odd-spin states, with the magnitude slowly increasing with the spin. For a triaxial potential, the level clustering in the γ band is opposite, and $S(I)$ oscillates between positive values for even-spin states and negative values for odd-spin states. In this case, the magnitude of $S(I)$ increases more rapidly with the spin, compared to the γ-soft potential [93].

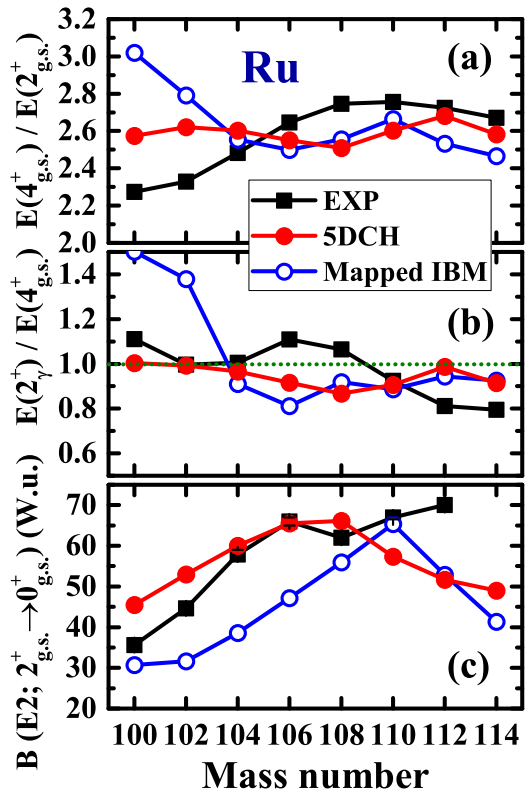

FIG. 5. Evolution of (a) $E(4^+_{g.s.})/E(2^+_{g.s.})$, (b) $E(2^+_\gamma)/E(4^+_{g.s.})$, and (c) $B(E2; 2^+_{g.s.} \to 0^+_{g.s.})$ values (in W.u.) with the mass number for Ru isotopes calculated by 5DCH-CDFT, in comparison with the available data [23,84] and theoretical results from the mapped IBM [15].

In Fig. 6, we plot the theoretical γ-band staggering parameters $S(I)$ for Ru isotopes, in comparison with the available experimental data. In general, the experimental staggering parameters are well reproduced by the 5DCH calculations, in particular, for low spins. For the isotopes $^{100-104}$Ru, the γ-band staggering parameters $S(I)$ present as the cases with deformed γ-soft potentials, namely, oscillating between negative values for even-spin states and positive values for odd-spin states. The deviation for the high-spin states in ^{100}Ru may be because the calculated PES is too stiff in the γ direction around the global minimum (cf. Fig. 1). Moving to ^{106}Ru, the phase of $S(I)$ at low spins is the same as in the case of the γ-soft potential but is inverted for $I \geqslant 8\ \hbar$. Therefore, it could be a transitional nucleus from the γ-soft to the triaxial deformed shape along increasing isospin. The nucleus ^{108}Ru has a γ-soft potential according to the experimental $S(I)$, while the calculated $S(I)$ demonstrates that this nucleus is similar to the neighboring ^{106}Ru as a transitional nucleus. The model probably overestimates the triaxiality of ^{108}Ru, which is also reflected in the too low γ bandhead 2^+_γ and too high interband $B(E2; 2^+_\gamma \to 2^+_{g.s.})$ in Fig. 3(e). For ^{110}Ru, although $S(4)$ is negative and $S(5)$ is positive, both of them are very close to 0. When $I \geqslant 6\hbar$, the $S(I)$ becomes negative for odd spins and positive for even spins, and considerable oscillation amplitudes are also observed. Thus, ^{110}Ru is close to the case of the γ-rigid shape [91]. Remarkable oscillations of $S(I)$ are observed in ^{112,114}Ru, indicating that they are triaxiality deformed.

The mixing of different intrinsic configurations in state $|\alpha I\rangle$ can be demonstrated from the distribution of K, the projection of angular momentum I on the third axis in the body-fixed frame:

$$N_K = 6 \int_0^{\pi/3} \int_0^{\infty} \left|\psi^I_{\alpha K}(\beta,\gamma)\right|^2 \beta^4 |\sin 3\gamma| d\beta d\gamma. \quad (6)$$

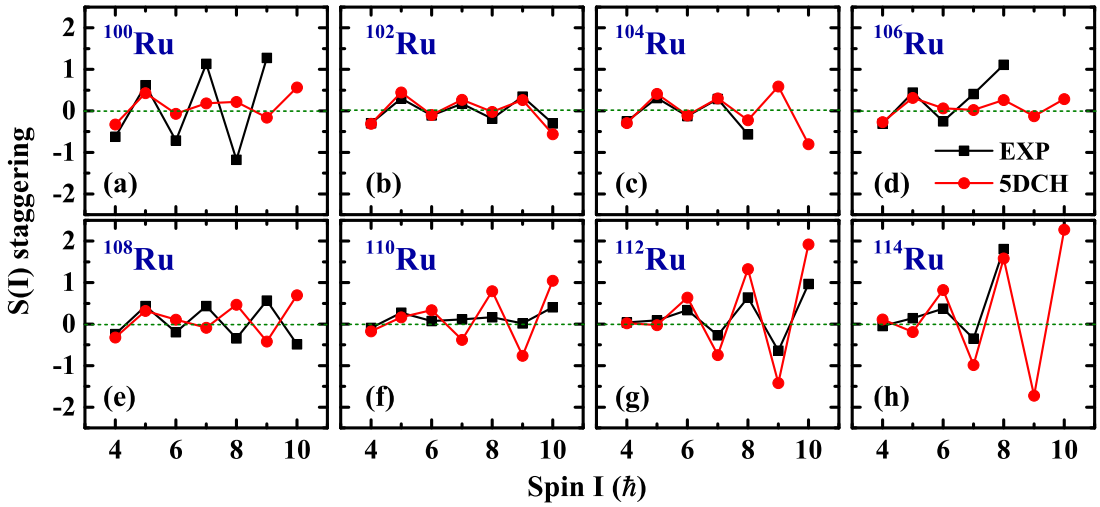

FIG. 6. Staggering parameters $S(I)$ of even-even $^{100-114}$Ru isotopes calculated by 5DCH-CDFT in comparison with the available data [84].

Figure 7 displays the distributions of K components in the collective wave functions for the 2^+, 4^+, 6^+, 8^+, and 10^+ states in the ground-state and γ bands of selected Ru isotopes: ^{100}Ru, ^{104}Ru, ^{110}Ru, and ^{112}Ru. In the cases of ^{100,104}Ru, $K = 0$ components are predominant in the wave functions for the yrast states, whereas the states comprising γ bands are dominated by $K = 2$ components. The mixing of $K = 0$ and $K = 2$ components is small for low-spin states, and thus the states are dominated by prolate configurations (cf. Fig. 8). For higher spin states, the mixing of K components is much stronger, indicating that the triaxial degree of freedom plays an important role in these states. For ^{110,112}Ru, the mixing of K components becomes remarkable for all the states and it is also notable that the $K > 2$ components are pronounced in the γ bands. This is strongly correlated with the triaxial deformed potentials of these isotopes (cf. Fig. 1) and also consistent with the oscillation behavior of $S(I)$ in Fig. 6.

The density distribution of the collective state, which takes the form

$$\rho_{I\alpha}(\beta,\gamma) = \sum_{K\in\Delta I} \left|\psi^I_{\alpha K}(\beta,\gamma)\right|^2 \beta^3, \tag{7}$$

with the normalization

$$\int_0^\infty \beta d\beta \int_0^{2\pi} \rho_{I\alpha}(\beta,\gamma)|\sin(3\gamma)|d\gamma = 1, \tag{8}$$

could provide further insight into the shape evolution with the spin and isospin. Here, taking ^{100}Ru, ^{104}Ru, ^{110}Ru, and ^{112}Ru as examples, the density distributions for the $0^+_{\text{g.s.}}$, $2^+_{\text{g.s.}}$, and 2^+_γ states are depicted in Fig. 8. For states 0^+ and 2^+, in the ground-state bands of ^{100,104,110,112}Ru, the peaks of collective wave functions are, in general, consistent with the global minima of the PESs, as shown in Fig. 1, while to some extent differences are observed because the masses of inertia are

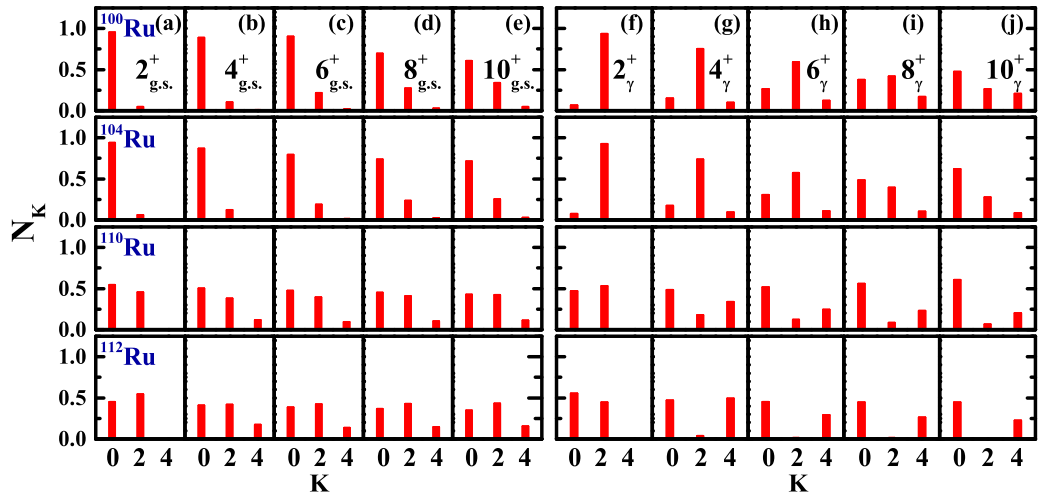

FIG. 7. Distributions of K components in the collective wave functions for the 2^+, 4^+, 6^+, 8^+, and 10^+ states in the ground-state and γ bands of ^{100,104,110,112}Ru.

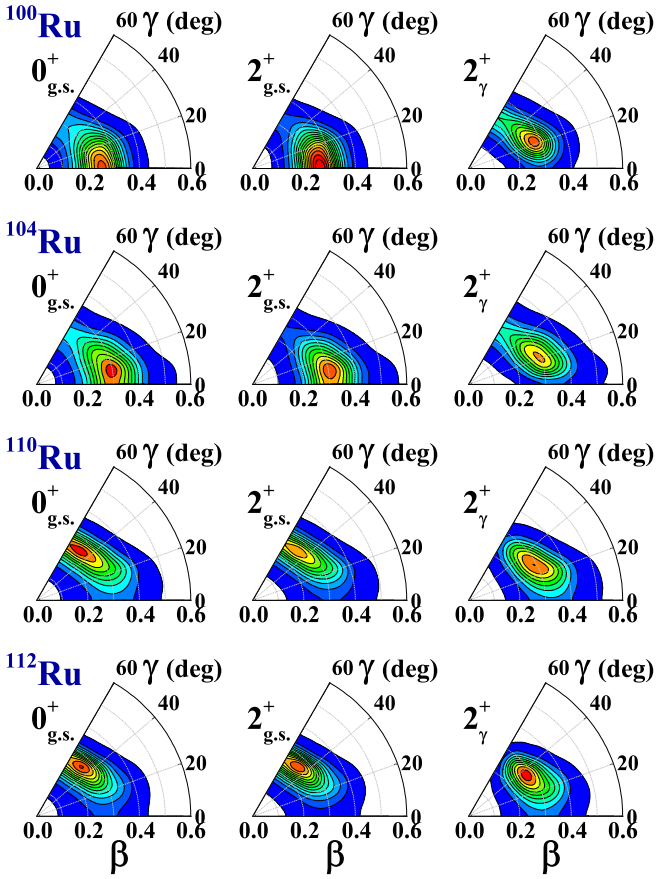

FIG. 8. Probability density distributions in the β-γ plane for the $0^+_{\rm g.s.}$, $2^+_{\rm g.s.}$, and 2^+_γ states in ^{100,104,110,112}Ru.

strongly deformation dependent. Weak triaxial deformations are predicted in states $0^+_{\rm g.s.}$ and $2^+_{\rm g.s.}$ of the ^{104,110,112}Ru isotopes. The collective wave functions of 2^+_γ are all concentrated in the region with $\gamma = 20^\circ$–40°, which demonstrates the importance of the triaxial degree of freedom in this mass region of Ru isotopes.

IV. SUMMARY

In this work, we have presented a microscopic and systematic beyond-mean-field investigation for the low-lying states in Ru isotopes around the $A \approx 100$ mass region. The excitation energies and transition strengths calculated from a five-dimensional collective Hamiltonian with parameters determined from the constrained triaxial CDFT calculations with the PC-PK1 functional reproduce the available data well. The microscopic potential energy surfaces exhibit transitions with increasing neutron number: from prolate ^{100}Ru to triaxial ^{114}Ru. The low-energy spectra, interband transition rates between the γ band and the ground-state band, and collective wave functions, as well as the characteristic collective observables $E(4^+_{\rm g.s.})/E(2^+_{\rm g.s.})$, $E(2^+_\gamma)/E(4^+_{\rm g.s.})$, and $B(E2; 2^+_{\rm g.s.} \to 0^+_{\rm g.s.})$ and γ-band staggerings, strongly support the onset of triaxiality in low-lying states of Ru isotopes around ^{110}Ru.

ACKNOWLEDGMENTS

Z.S. is indebted to Prof. Jie Meng for constructive guidance and valuable suggestions. Fruitful discussions with and critical readings from Dr. Shuangquan Zhang and Dr. Pengwei Zhao are gratefully acknowledged. This work was partly supported by the National Natural Science Foundation of China (Grants No. 11475140, No. 11375015, No. 11461141002, No. 11335002, and No. 11621131001) and the Chinese Major State 973 Program (Grant No. 2013CB834400).

[1] A. Bohr and B. R. Mottelson, *Nuclear Structure, Vol. II* (Benjamin, New York, 1975).
[2] S. Frauendorf and J. Meng, Nucl. Phys. A **617**, 131 (1997).
[3] J. Meng, J. Peng, S. Q. Zhang, and S.-G. Zhou, Phys. Rev. C **73**, 037303 (2006).
[4] K. Starosta, T. Koike, C. Chiara, D. Fossan, D. LaFosse, A. Hecht, C. Beausang, M. Caprio, J. Cooper, R. Krücken *et al.*, Phys. Rev. Lett. **86**, 971 (2001).
[5] S. W. Ødegård, G. B. Hagemann, D. R. Jensen, M. Bergström, B. Herskind, G. Sletten, S. Törmänen, J. N. Wilson, P. O Tjøm, I. Hamamoto, K. Spohr, H. Hubel, A. Gorgen, G. Schonwasser, A. Bracco, S. Leoni, A. Maj, C. M. Petrache, P. Bednarczyk, and D. Curien, Phys. Rev. Lett. **86**, 5866 (2001).
[6] P. Sarriguren, R. Rodríguez-Guzmán, and L. M. Robledo, Phys. Rev. C **77**, 064322 (2008).
[7] L. M. Robledo, R. Rodríguez-Guzmán, and P. Sarriguren, J. Phys. G **36**, 115104 (2009).
[8] Z. P. Li, T. Nikšić, D. Vretenar, and J. Meng, Phys. Rev. C **81**, 034316 (2010).
[9] Y. Toh, C. J. Chiara, E. A. McCutchan, W. B. Walters, R. V. F. Janssens, M. P. Carpenter, S. Zhu, R. Broda, B. Fornal, B. Kay *et al.*, Phys. Rev. C **87**, 041304 (2013).
[10] J. M. Yao, K. Hagino, Z. P. Li, J. Meng, and P. Ring, Phys. Rev. C **89**, 054306 (2014).
[11] T. Nikšić, P. Marević, and D. Vretenar, Phys. Rev. C **89**, 044325 (2014).
[12] J. J. Sun, Z. Shi, X. Q. Li, H. Hua, C. Xu, Q. B. Chen, S. Q. Zhang, C. Y. Song, J. Meng, X. G. Wu *et al.*, Phys. Lett. B **734**, 308 (2014).
[13] G. H. Bhat, W. A. Dar, J. A. Sheikh, and Y. Sun, Phys. Rev. C **89**, 014328 (2014).
[14] J. Xiang, J. M. Yao, Y. Fu, Z. H. Wang, Z. P. Li, and W. H. Long, Phys. Rev. C **93**, 054324 (2016).
[15] K. Nomura, R. Rodríguez-Guzmán, and L. M. Robledo, Phys. Rev. C **94**, 044314 (2016).
[16] J. Stachel, N. Kaffrell, E. Grosse, H. Emling, H. Folger, R. Kulessa, and D. Schwalm, Nucl. Phys. A **383**, 429 (1982).
[17] J. Stachel, N. Kaffrell, N. Trautmann, K. Broden, G. Skarnemark, and D. Eriksen, Z. Phys. A **316**, 105 (1984).
[18] J. Äystö, P. Jauho, Z. Janas, A. Jokinen, J. Parmonen, H. Penttilä, P. Taskinen, R. Béraud, R. Duffait, A. Emsallem *et al.*, Nucl. Phys. A **515**, 365 (1990).

[19] I. Deloncle, A. Bauchet, M.-G. Porquet, M. Girod, S. Peru, J.-P. Delaroche, A. Wilson, B. Gall, F. Hoellinger, N. Schulz *et al.*, Eur. Phys. J. A **8**, 177 (2000).

[20] J. A. Shannon, W. R. Phillips, J. L. Durell, B. J. Varley, W. Urban, C. J. Pearson, I. Ahmad, C. J. Lister, L. R. Morss, K. L. Nash *et al.*, Phys. Lett. B **336**, 136 (1994).

[21] S. J. Zhu, Y. X. Luo, J. H. Hamilton, J. O. Rasmussen, A. V. Ramayya, J. K. Hwang, H. B. Ding, X. L. Che, Z. Jiang, P. M. Gore *et al.*, Prog. Part. Nucl. Phys. **59**, 329 (2007).

[22] Y. X. Luo, S. J. Zhu, J. H. Hamilton, J. O. Rasmussen, A. V. Ramayya, C. Goodin, K. Li, J. K. Hwang, D. Almehed, S. Frauendorf *et al.*, Phys. Lett. B **670**, 307 (2009).

[23] D. T. Doherty, J. M. Allmond, R. V. F. Janssens, W. Korten, S. Zhu, M. Zielińska, D. C. Radford, A. D. Ayangeakaa, B. Bucher, J. C. Batchelder *et al.*, Phys. Lett. B **766**, 334 (2017).

[24] P. Möller, R. Bengtsson, B. G. Carlsson, P. Olivius, and T. Ichikawa, Phys. Rev. Lett. **97**, 162502 (2006).

[25] P. Möller, R. Bengtsson, B. Carlsson, P. Olivius, T. Ichikawa, H. Sagawa, and A. Iwamoto, At. Data Nucl. Data **94**, 758 (2008).

[26] B. Sorgunlu and P. Van Isacker, Nucl. Phys. A **808**, 27 (2008).

[27] M. Böyükata, P. Van Isacker, and I. Uluer, J. Phys. G **37**, 105102 (2010).

[28] J. Q. Faisal, H. Hua, X. Q. Li, Y. Shi, F. R. Xu, H. L. Liu, Y. L. Ye, and D. X. Jiang, Phys. Rev. C **82**, 014321 (2010).

[29] K. Nomura, N. Shimizu, and T. Otsuka, Phys. Rev. C **81**, 044307 (2010).

[30] A. Bhat, A. Bharti, and S. Khosa, Int. J. Mod. Phys. E **21**, 1250030 (2012).

[31] H. Abusara, S. Ahmad, and S. Othman, Phys. Rev. C **95**, 054302 (2017).

[32] C. L. Zhang, G. H. Bhat, W. Nazarewicz, J. A. Sheikh, and Y. Shi, Phys. Rev. C **92**, 034307 (2015).

[33] Q. B. Chen, N. Kaiser, U.-G. Meißner, and J. Meng, Eur. Phys. J. A **53**, 204 (2017).

[34] P. Ring, Prog. Part. Nucl. Phys. **37**, 193 (1996).

[35] D. Vretenar, A. Afanasjev, G. Lalazissis, and P. Ring, Phys. Rep. **409**, 101 (2005).

[36] J. Meng, H. Toki, S. G. Zhou, S. Q. Zhang, W. H. Long, and L. S. Geng, Prog. Part. Nucl. Phys. **57**, 470 (2006).

[37] J. Meng, J. Peng, S. Q. Zhang, and P. W. Zhao, Front. Phys. **8**, 55 (2013).

[38] J. Meng, *Relativistic Density Functional for Nuclear Structure* (World Scientific, Singapore, 2016).

[39] J. Meng, K. Sugawara-Tanabe, S. Yamaji, and A. Arima, Phys. Rev. C **59**, 154 (1999).

[40] T. S. Chen, H. F. Lü, J. Meng, S. Q. Zhang, and S.-G. Zhou, Chin. Phys. Lett. **20**, 358 (2003).

[41] S.-G. Zhou, J. Meng, and P. Ring, Phys. Rev. Lett. **91**, 262501 (2003).

[42] H. Z. Liang, J. Meng, and S.-G. Zhou, Phys. Rep. **570**, 1 (2015).

[43] W. H. Long, J. Meng, N. Van Giai, and S.-G. Zhou, Phys. Rev. C **69**, 034319 (2004).

[44] W. Zhang, J. Meng, S. Q. Zhang, L. S. Geng, and H. Toki, Nucl. Phys. A **753**, 106 (2005).

[45] P. W. Zhao, Z. P. Li, J. M. Yao, and J. Meng, Phys. Rev. C **82**, 054319 (2010).

[46] W. Zhang, Z. P. Li, and S. Q. Zhang, Phys. Rev. C **88**, 054324 (2013).

[47] J. Meng and P. Ring, Phys. Rev. Lett. **77**, 3963 (1996).

[48] J. Meng and P. Ring, Phys. Rev. Lett. **80**, 460 (1998).

[49] J. Meng, H. Toki, J. Y. Zeng, S. Q. Zhang, and S.-G. Zhou, Phys. Rev. C **65**, 041302 (2002).

[50] J. Meng and S.-G. Zhou, J. Phys. G **42**, 093101 (2015).

[51] H. Z. Liang, N. Van Giai, and J. Meng, Phys. Rev. Lett. **101**, 122502 (2008).

[52] H. Z. Liang, N. V. Giai, and J. Meng, Phys. Rev. C **79**, 064316 (2009).

[53] P. W. Zhao, S. Q. Zhang, J. Peng, H. Z. Liang, P. Ring, and J. Meng, Phys. Lett. B **699**, 181 (2011).

[54] P. W. Zhao, J. Peng, H. Z. Liang, P. Ring, and J. Meng, Phys. Rev. Lett. **107**, 122501 (2011).

[55] P. W. Zhao, J. Peng, H. Z. Liang, P. Ring, and J. Meng, Phys. Rev. C **85**, 054310 (2012).

[56] P. W. Zhao, N. Itagaki, and J. Meng, Phys. Rev. Lett. **115**, 022501 (2015).

[57] P. W. Zhao, S. Q. Zhang, and J. Meng, Phys. Rev. C **92**, 034319 (2015).

[58] P. W. Zhao, Phys. Lett. B **773**, 1 (2017).

[59] P. W. Zhao, L. S. Song, B. Sun, H. Geissel, and J. Meng, Phys. Rev. C **86**, 064324 (2012).

[60] P. W. Zhao, S. Q. Zhang, and J. Meng, Phys. Rev. C **89**, 011301 (2014).

[61] T. Nikšić, Z. P. Li, D. Vretenar, L. Próchniak, J. Meng, and P. Ring, Phys. Rev. C **79**, 034303 (2009).

[62] Z. P. Li, T. Nikšić, D. Vretenar, J. Meng, G. A. Lalazissis, and P. Ring, Phys. Rev. C **79**, 054301 (2009).

[63] T. Nikšić, D. Vretenar, and P. Ring, Prog. Part. Nucl. Phys. **66**, 519 (2011).

[64] S. Quan, Q. Chen, Z. P. Li, T. Nikšić, and D. Vretenar, Phys. Rev. C **95**, 054321 (2017).

[65] Z. P. Li, C. Y. Li, J. Xiang, J. M. Yao, and J. Meng, Phys. Lett. B **717**, 470 (2012).

[66] Z. H. Wang, J. Xiang, W. H. Long, and Z. P. Li, J. Phys. G **42**, 045108 (2015).

[67] Z. P. Li, T. Nikšić, D. Vretenar, and J. Meng, Phys. Rev. C **80**, 061301 (2009).

[68] Z. P. Li, J. M. Yao, D. Vretenar, T. Nikšić, H. Chen, and J. Meng, Phys. Rev. C **84**, 054304 (2011).

[69] J. Xiang, Z. P. Li, Z. X. Li, J. M. Yao, and J. Meng, Nucl. Phys. A **873**, 1 (2012).

[70] Y. Fu, H. Mei, J. Xiang, Z. P. Li, J. M. Yao, and J. Meng, Phys. Rev. C **87**, 054305 (2013).

[71] Y. Y. Wang, Z. Shi, Q. B. Chen, S. Q. Zhang, and C. Y. Song, Phys. Rev. C **93**, 044309 (2016).

[72] Z. P. Li, T. Nikšić, D. Vretenar, P. Ring, and J. Meng, Phys. Rev. C **81**, 064321 (2010).

[73] Q. B. Chen, S. Q. Zhang, P. W. Zhao, R. V. Jolos, and J. Meng, Phys. Rev. C **87**, 024314 (2013).

[74] Q. B. Chen, S. Q. Zhang, P. W. Zhao, R. V. Jolos, and J. Meng, Phys. Rev. C **94**, 044301 (2016).

[75] Q. B. Chen, S. Q. Zhang, P. W. Zhao, and J. Meng, Phys. Rev. C **90**, 044306 (2014).

[76] Q. B. Chen, S. Q. Zhang, and J. Meng, Phys. Rev. C **94**, 054308 (2016).

[77] L. Próchniak, K. Zajac, K. Pomorski, S. Rohoziński, and J. Srebrny, Nucl. Phys. A **648**, 181 (1999).

[78] J.-P. Delaroche, M. Girod, J. Libert, H. Goutte, S. Hilaire, S. Péru, N. Pillet, and G. F. Bertsch, Phys. Rev. C **81**, 014303 (2010).

[79] D. Inglis, Phys. Rev. **103**, 1786 (1956).

[80] S. Beliaev, Nucl. Phys. **24**, 322 (1961).

[81] M. Girod and B. Grammaticos, Nucl. Phys. A **330**, 40 (1979).
[82] M. Wang, G. Audi, F. Kondev, W. Huang, S. Naimi, and X. Xu, Chin. Phys. C **41**, 030003 (2017).
[83] I. Angeli and K. Marinova, At. Data Nucl. Data **99**, 69 (2013).
[84] http://www.nndc.bnl.gov/ensdf/.
[85] T. Nikšić, D. Vretenar, and P. Ring, Phys. Rev. C **78**, 034318 (2008).
[86] In the present work, the data for ^{104}Ru are taken from the evaluated database of the National Nuclear Data Center [84], while in Ref. [14] we used the data from http://ie.lbl.gov/TOI2003/index.asp.
[87] Y. Tian, Z. Ma, and P. Ring, Phys. Lett. B **676**, 44 (2009).
[88] Q. S. Zhang, Z. M. Niu, Z. P. Li, J. M. Yao, and J. Meng, Front. Phys. **9**, 529 (2014).
[89] K. Q. Lu, Z. X. Li, Z. P. Li, J. M. Yao, and J. Meng, Phys. Rev. C **91**, 027304 (2015).
[90] Z. P. Li, T. Nikšić, P. Ring, D. Vretenar, J. M. Yao, and J. Meng, Phys. Rev. C **86**, 034334 (2012).
[91] A. S. Davydov and G. F. Filippov, Nucl. Phys. **8**, 237 (1958).
[92] N. V. Zamfir and R. F. Casten, Phys. Lett. B **260**, 265 (1991).
[93] E. A. McCutchan, D. Bonatsos, N. V. Zamfir, and R. F. Casten, Phys. Rev. C **76**, 024306 (2007).